Bioelectrochemistry 120 (2018) 66–75

Contents lists available at ScienceDirect

Bioelectrochemistry

journal homepage: www.elsevier.com/locate/bioelechem

Peptide-based biosensors: From self-assembled interfaces to molecular probes in electrochemical assays☆

Mihaela Puiu [a], Camelia Bala [a,b,*]

[a] R&D Center LaborQ, University of Bucharest, 4-12 Regina Elisabeta Blvd., 030018 Bucharest, Romania
[b] Department of Analytical Chemistry, University of Bucharest, 4-12 Regina Elisabeta Blvd., 030018 Bucharest, Romania

ARTICLE INFO

Article history:
Received 28 October 2017
Received in revised form 21 November 2017
Accepted 21 November 2017
Available online 23 November 2017

Keywords:
Biosensor
Peptide
Electrochemical assays
Redox tag

ABSTRACT

Redox-tagged peptides have emerged as functional materials with multiple applications in the area of sensing and biosensing applications due to their high stability, excellent redox properties and versatility of biomolecular interactions. They allow direct observation of molecular interactions in a wide range of affinity and enzymatic assays and act as electron mediators. Short helical peptides possess the ability to self-assemble in specific configurations with the possibility to develop in highly-ordered, stable 1D, 2D and 3D architectures in a hierarchical controlled manner. We provide here a brief overview of the electrochemical techniques available to study the electron transfer in peptide films with particular interest in developing biosensors with immobilized peptide motifs, for biological and clinical applications.

Contents

1. Introduction

Peptides are probably the most versatile tools in the development of supramolecular and flexible frameworks due to their inherent ability to self-assemble in highly-ordered 1D, 2D and 3D structures. Due to their tunable physio-chemical properties, peptides are able to fold in compact structural motifs shaping nanosized architectures in monolayers, bilayers, fibers, micelles, tubes, and strips [1,2]. Peptide self-assembly is driven by noncovalent intermolecular interactions (electrostatic, hydrogen bonding, hydrophobic, aromatic π-stacking and van der Waals) through molecular recognition [3,4]. The secondary structure of peptides (α- and, 3_{10} helices, β-sheets and β-hairpins) can be easily modulated by engineering the amino acid (AA) sequence in order to optimize the

Abbreviations: AA, amino acid; Fc, ferrocene; MB, methylene blue; AMP, antimicrobial peptide; CPP, cell-penetrating peptide; Aib, α-aminoisobutyric acid; SAM, self-assembled monolayers; ADNT, aromatic dipeptide nanotubes; ET, electron transfer; CV, cyclic voltammetry; SWV, square wave voltammetry; ACV, alternating current voltammetry; DPV, differential pulse voltammetry; EIS, electrochemical impedance spectroscopy; SWCNT, single-walled carbon nanotube; DWCNT, double-walled carbon nanotube; EGFR, epidermal growth factor receptor; DGP, deamidated gliadin peptide; PDDA, poly(diallyl dimethyl) ammonium chloride; PNW, peptide nanowire; AuNP, gold nanoparticle; GN, grapheme nanoparticle.

☆ This is a part of VSI: BES 2017.

* Corresponding author at: Department of Analytical Chemistry, University of Bucharest, 4-12 Regina Elisabeta Blvd., 030018 Bucharest, Romania.
E-mail address: camelia.bala@chimie.unibuc.ro (C. Bala).

https://doi.org/10.1016/j.bioelechem.2017.11.009
1567-5394/

interactions between adjacent peptides [5,6]. The helical conformations provide intrinsic electron transfer and conductive properties, leading to the idea that peptide scaffolds might be used for building materials with electronic/photoelectronic functions [6]. Moreover, short peptides (up to 10 AA residues) [3,7] can be easily obtained by standard synthesis methods, avoiding complex, laborious and time-consuming procedures, as in the case large proteins [2,8]. They are also biocompatible, and therefore excellent candidates for stabilizing labile macromolecules such as enzymes, antibodies and nucleic acids used in biosensors and bionanodevices [2,9]. Peptide-based biosensors have been developed for the detection of various analytes, including cells [10] proteins [11] ions [12,13] or small molecules.

The 20 natural amino acids (Fig. 1) are the building blocks in peptide synthesis. All natural amino acids, except glycine (G), are chiral adopting the $_{L}$-configuration. They have the same basic structure and vary only in the R-group at the central carbon (C_{α}) position of the molecule. Peptides adopt specific configurations, depending on which R-groups are near one another in a peptide chain [14]. AA sequences ensure the primary structure, usually designated with one-letter code (Fig. 1).

The nature of the R group dictates the peculiarity of each AA residue, which can be categorised as hydrophobic, hydrophilic, charged, or "other" [15,16]. The hydrophobic residues can be divided in two groups: the aliphatic residues, A, I, L, M, V and the aromatic residues F, W and Y. The aliphatic residues generally provide a hydrophobic environment. Aromatic residues are usually involved in π–π stacking, where p-orbitals in π-conjugated system overlap [1,6]. These interactions are mainly involved in peptide folding [17,18]. The hydrophilic, polar residues participate to hydrogen bonding, either via OH (S, T) or CONH (N, Q) groups. The ionisable residues can be positively charged, H, K, R, and have pK_a values of 6.5, 10 and 12, respectively, or negatively charged, D, E, and both have similar pK_a of 4.4 [14]. The oppositely charged residues may promote the formation of peptide assemblies through their electrostatic attraction, while equal charges prevent

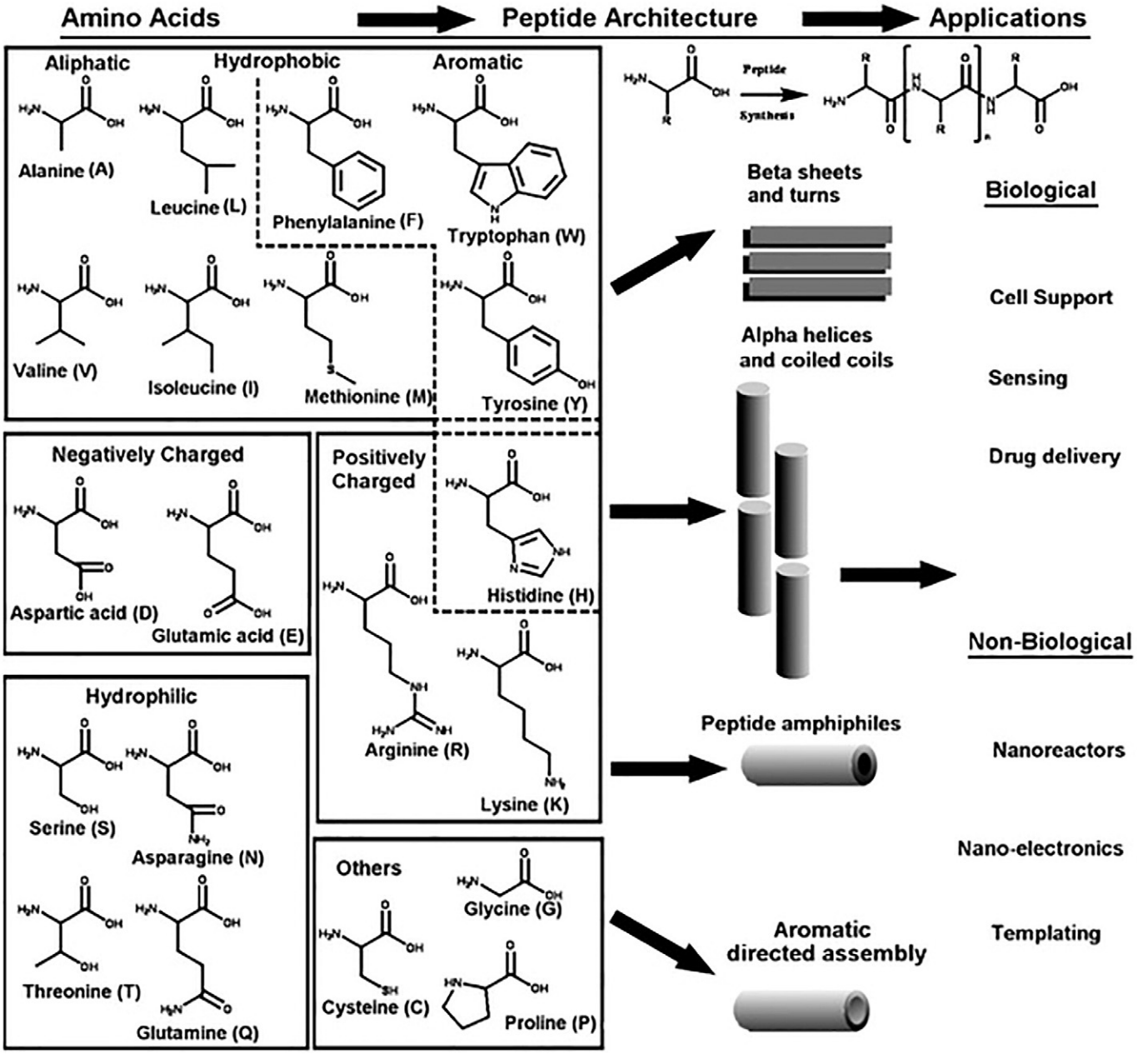

Fig. 1. Basic structures of amino acids are displayed along with their common name and the one letter abbreviations. The main architectures derived from peptide sequencing are presented with their potential applications in nano-biomedicine and nano-electronics. Reproduced from [14] with permission of RSC Publishing.

assembly through electrostatic repulsion [19]. The "other" category contains several specific residues, that either offer structural modifications such as bends in peptide chains, or sites for chemical modification [14]. The presence of two hydrogen atoms in glycine (G) removes the steric hindrance imposed by the R-group, and provides a higher degree of flexibility of the peptide sequence compared to other amino acids. Proline residues introduce structural rigidity due to the blocked conformation caused by the side chain being covalently linked to the amino terminus. Cysteine (C) can be used to bind to gold surfaces [3,14]. Serine (S), threonine (T) and are suitable for chemical or enzymatic modification, while repeated sequences of histidine (H) are able bind metal ions such as Ni^{2+} [20] or Cu^{2+} [12,13].

2. Interfacing electrochemical transducers with peptidic elements

There are plenty different approaches to immobilize peptidic elements onto surfaces, from physical absorption to covalent attachment to a self-assembled monolayer [20]. Gold-thiol chemistry can be also used to prepare self-assembled monolayers (SAMs) of short synthetic peptides on gold surfaces [21,22]. However, these approaches require conjugation of a redox reporter such as ferrocene (Fc) [7,23] or methylene blue (MB) [24,25], as peptides do not directly generate measurable electrochemical signals in response to a binding event [26]. Therefore, label-free detection would be a challenging task to achieve for peptide-based assays, either if peptides are working as supporting self- assembled layers, or are mimicking a recognition element for a specific target. Moreover, the selectivity of assays with peptides as recognition elements should be carefully optimized due to the semi-selective binding nature of peptides [27]. Many peptides displayed significant binding affinity toward several different cells/molecules [26]. The peptide elements for biosensing approaches are selected according to the assay formats and analytical purpose:

- Short peptides from random phage display: in this case the peptides are randomly selected from large and often pre-existing and commercially available phage display libraries, with no design elements [28].
- Peptide receptors for ligand sensing: artificial peptide receptors can be obtained from the reduction of the known sequence of a natural receptor down to a synthesizable and stable sequence [29]. On the other hand, a binding site can be created over a designed, stable peptide framework.
- Peptide ligands for receptor sensing: short peptides can also be used as specific elements for the detection of their own receptors. Therefore, antimicrobial peptides (AMPs) [27] and cell-penetrating peptides (CPPs) [30], which are able to interact with cell-surface elements, are used for sensing bacterial cells, antigenic peptide sequences for antibody binding, and peptide substrates for enzyme detection [29]. Electrochemical peptide-based sensors are usually developed following a "bottom-up" strategy, either if it is about interfacing the transducer with peptide SAMs or attaching a peptide recognition element on an already built-up alkyl-thiolated SAM [31]. The bottom-up fabrication refers to the arrangement of smaller components into a larger or more complex assembly [32] (Fig. 2). By contrast, the top-down fabrication is defined as the development of organized structures either by etching down a bulk material or by manipulating components into specific locations.

While the bottom-up approach builds-up nanomaterials from small blocks like atoms or molecules, the top-down approach produces nanostructures by deconstructing larger materials with the use of lithographic tools (i.e., physical top-down) or through chemical-based processes (i.e., chemical top-down) [33]. Amphiphilic and aromatic peptides are the most used building-block candidates for "smart

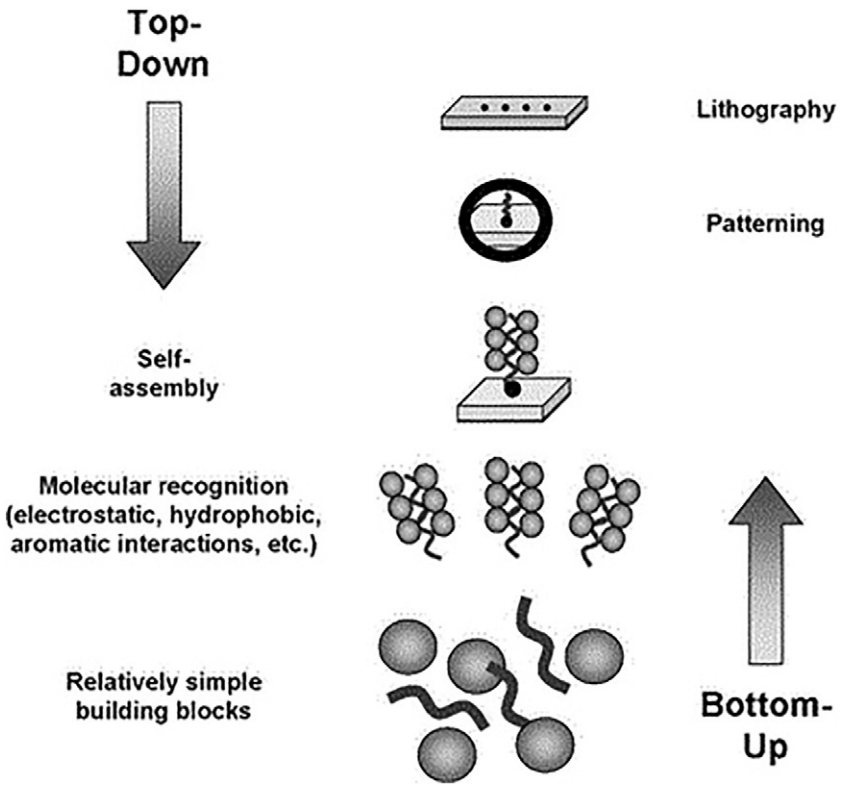

Fig. 2. Comparison between "top-down" and "bottom-up" techniques. The top-down procedure is based on the patterning of assemblies by lithographic definition. The "bottom-up" approach is based on the interaction of simple building blocks to form a well-ordered assembly by means of molecular recognition and self-assembly. Reproduced from [8] with permission of RSC Publishing.

materials" whose development involves self-assembling. For example, using diphenylalanine, *Gazit* and co-workers have developed aromatic dipeptide nanotubes (ADNTs) ranging between 50 and 300 nm in diameter and up to microns in length [8,32]. There are various systems based on amphiphilic molecules which have been exploited in combination with top-down methods. Bolaamphiphiles, for example, consist of two hydrophilic groups connected by a hydrophobic linker segment [34]. *Matsui* and co-workers have developed a bolaamphiphile system dissolved in sodium hydroxide that self-assembles into 100 nm diameter nanotubes upon pH reduction [32,33]. In this case, self-assembly results from hydrophobic associations of the alkyl chains due to charge neutralization when the carboxylic acid head groups become protonated. These nanotubes have been patterned into precise locations on gold surfaces coated with 1-octadecanethiol SAMs [35]. These materials can be used further for the controlled immobilization of proteins in affinity assays [34]. Nevertheless, it is crucial to provide insights into the mechanisms governing the electron transfer in electrochemical peptide-based sensors regardless the manner of transducer's functionalization. Here, the ability of several peptides to mediate the electron transfer (ET) between a redox center and the electrode surface, in a direction-dependent manner, is to be exploited.

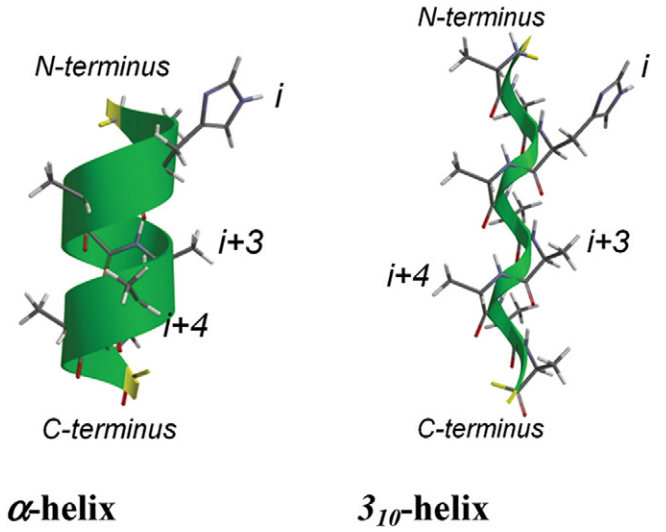

Fig. 3. Helical α- and 3_{10}-conformations based on a polyalanine/histidine 9-mer peptide showing the relative positions of *i*, $i + 3$, and $i + 4$ residues in the helix. Reproduced from [44] with permission of RSC Publishing.

3. Electron transfer through peptide films

The ability to form tightly packed monolayers, which is crucial for an efficient ET through a peptide bridge, depends on the length of the peptides and their 3D-structure. Short peptides may populate several conformations, being very flexible and rapidly inter-converted between the different conformers [36,37]. Consequently, they form loosely packed films with large degrees of inhomogeneity and up to 15% vacant gold sites [36]. On the contrary, longer helical peptides form well-ordered and densely packed films [38]. The capability to form tightly packed SAMs depends not only on the length of the peptide primary structure, but also on the type of secondary structure attained by the peptide chains and on the presence of aromatic groups [39].

The α-helix is the most observed secondary structure in peptides and proteins, where the dihedral angles ω, Φ and Ψ have the values of 180°, −57° and −47°, respectively. In the case of the 3_{10} helix the dihedral angles are 180°, −49° and −27° [22,40]. The basic difference between a 3_{10} helix and an α-helix resides in the manner in which the backbone hydrogen-bonding network of the two helices is established; in α-helices, the carbonyl group of residue *i* interacts with the nitrogen from the amide group in residue $i + 4$ [15,41] yielding the following characteristics: 3.6 residues per turn and consecutive residues making an angle of 100° around the helical axis, a helical rise per residue of 1.5 Å, and a helical pitch of 5.4 Å [42]. By contrast, in 3_{10} helix, the carbonyl group in residue *i* and the nitrogen of the amide group in residue $i + 3$ are hydrogen bonded [43]. Canonical 3_{10} helices have 3 residues per turn, with an angle of 120° between consecutive residues, a helical rise per residue of 1.93–2.0 Å, and a helical pitch of 5.8–6 Å. Thus, the 3_{10} helix is longer and thinner than the α-helix with the same number of residues [15,44] (Fig. 3).

Gatto and co-workers have demonstrated that six residues-long peptide containing α-aminoisobutyric acid (Aib) residues can be folded in helical conformations [45]. Other works reported that oligopeptides containing up to 8 residues, modified at $N_{terminus}$ with a lipoyl moiety able to form densely packed monolayers [24,37,45], mainly due to their helical secondary structure. The molecular dipole moment greatly influences the rate of the peptide-mediated ET [7,37], especially in the α- helical peptides, which exhibit a large macrodipole moment (approximately 3.5 D per residue) [22], oriented parallel to the molecular axis. Of special interest are also 3_{10}-helices, which exhibit high dipole moments as well, leading to the formation of an effective positive charge at the $N_{terminus}$ and a negative charge at $C_{terminus}$.

It is now widely accepted that the charge transfer through the peptide spacer is strongly affected by the separation between acceptor (A) and donor (D) sites, the characteristics of the peptide backbone along with its secondary structure and the resulting flexibility [36,46]. Since the separation between the donor and acceptor sites is relatively large, the electronic coupling between them is expected to be weak [23]. Therefore, ET occurs in a nonadiabatic regime, and its rate constant (k_{ET}) can be described with Fermi's golden rule [47]:

$$k_{ET} = \left(\frac{2\pi}{h}\right)|H_{DA}|^2(FC) \tag{1}$$

where H_{DA} is the electronic coupling matrix element between D and A, and FC denotes the Franck-Condon factor, which express the contribution of the nuclear reorganization to the ET rate [47]:

$$FC = \frac{1}{(4\pi\lambda k_B T)^{1/2}}\ exp\left(-\frac{\left(\Delta G^0 + \lambda\right)^2}{4\pi\lambda k_B T}\right) \tag{2}$$

In Eq. (2), λ represents the reorganization energy (the energy required to reorient all atoms from equilibrium state to the product state), ΔG^0 is the Gibbs free energy of ET reaction k_B is the Boltzmann constant, and *T* is the absolute temperature.

The factors that control the rate of these processes have been investigated with photo-physical techniques and the results were analyzed using various methods, including Marcus–Hush theory of electron tunneling [7,45,48]. Currently, there are two major mechanisms debating the distance dependence of ET in peptide models: a bridge-assisted superexchange and an electron-hopping mechanism [22,49]. According to the hoping mechanism, the electron temporarily resides on the bridge for a short time during its passing from the donor to the acceptor and involves sequential tunneling steps between its neighbouring units, which act as hopping sites [22]; in the superexchange mechanism, the conjugated bridge only serves as a medium to pass the electron between the donor and acceptor [36,40]. In a superexchange mechanism, the ET rate exhibits an exponentially distance dependence, while a linear distance relationship is expected for a hopping mechanism [36]. Since $|H_{DA}|$ depends on the overlap of the electronic wave functions of the donor and the acceptor and thus upon the distance *r*, on which electron tunneling takes place [50], it can be expressed as:

$$|H_{DA}|^2 = |H_{DA}|^2_{(r=r_0)}\ exp(-\beta(r-r_0)) \tag{3}$$

Where β is a damping factor whose value is typically <1.2 $Å^{-1}$ for through-space ET [47].

If $r\text{-}r_0 = l_{DA}$ is the distance separating the donor from the acceptor, then the ET rate constant follows an exponential distance dependence, according to [51]:

$$k_{ET} \propto exp(-\beta l_{DA}) \quad (4)$$

The tunneling-pathway model predicts decay factors of 1.0 and 1.3 $Å^{-1}$ for β-strand and α-helix conformations, respectively [52]. Due to the sharp exponential decay of the ET rate constant with increasing length of the bridge, the superexchange mechanism is limited to short distances. The driving force is defined as the difference in the redox potentials of the donor and acceptor (Fermi level in the case of metal). For low driving forces, the upper limit for tunneling is around 2 nm [52]. Nevertheless, in some proteins, the electron transfer occurs over long distances, reaching up to 3.5 nm. Here the experimental values of the damping factors are often below 1.0 $Å^{-1}$ [7]. The multistep mechanism involves certain units/functional groups, which can be reversibly oxidized or reduced, and act as relay stations, where the electron/hole resides for a short time before it continues to the next hopping step [23,53]. In such cases, the distance dependence is much weaker compared with superexchange mechanism, and can be depicted as [54]:

$$k_{ET} \propto \frac{1}{N}\ exp\left(-\frac{E_a}{k_B T}\right) \quad (5)$$

where N is the number of hopping sites, and E_a is the activation energy of ET reaction. Both hopping and superexchange mechanisms may contribute in an ET system. There is an extensive body of work dedicated to study of ET through peptide films, but of particular interest for electrochemical applications are SAMs of helical peptides (α and 3_{10} configurations) [23,45,55]. The 3_{10}-helix is presumed to be more conductive than the α-helix (due to the increased number, $i \rightarrow i+3$ versus $i \rightarrow i+4$, respectively, and, therefore stronger intramolecular H-bonded). Thus, the 3_{10} conformation may be a potential candidate for the ET active conformer, and the formation rate of this conformation (which is sluggish in close-packed SAMs compared to that in solutions) controls the overall ET rate in helical peptide SAMs [56].

4. Electrochemical methods in peptide-based assays

Electrochemical methods have been extensively used for studying the electron transfer mediated by peptide bridges [21,49,55,57]. For this purpose, a three-electrode cell is used, with the peptide-modified gold electrode as working electrode. In this manner, the redox tag can be separated from the electrode surface by a certain distance, defined by the thickness of the adsorbed film. Upon applying the potential, the electron flow occurs between the redox tag and the electrode's surface, and the overall process is mediated by the molecules forming the monolayer [23]. Thus, ET may occur through a two-component SAM having both electroactive molecules with a covalently attached redox tags and passive diluent molecules [24,40,58]. The results obtained to-date clearly show the importance of the monolayers' design for the electrochemical studies of mediated electron transfer, particularly when considering peptides with a covalently attached redox center, such as Fc [22] or MB [59]. Thus, the optimal design of a redox-peptide system requires co-adsorption of diluent molecules, with adjusted lengths in order to eliminate the interactions between the charged redox centers. Both ET mechanisms are available but the dominant one is switchable, depending on the D/A distance and the reaction driving force of the molecular system. When the electron-transfer distance is short or the driving force is large, tunneling mechanism is preponderant [7]. One-component electroactive monolayers usually exhibit significantly faster standard rate constants, compared with two-component monolayers containing diluent molecules [60]. In a one-component system, the electroactive centers are closer to each other, and electron hopping between them is possible. Also, stronger electrostatic interactions between charged sites may contribute to the measured rate constant [48]. In addition, the molecular motion of the peptide backbone may be hindered by tight molecular packing in highly compact layers. Restricted molecular dynamics may hamper or slow down the electron transfer [36]. In these conditions it is difficult to distinguish a purely electrochemical response from an electrochemical signal distorted by the molecular motion of the molecules on the surface. For example, the time scale of the electron movement from a ferrocene Fc tag to the gold surface through a peptide bridge is often slower than the time scale of molecular motions, especially when external electric field are applied, forcing charged molecule to align itself within the field gradient [36,56,58,61].The most commonly used electrochemical methods to measure k_{ET} using redox-modified SAM systems are cyclic voltammetry (CV), alternating current (AC), square wave (SW), differential pulse (DP) voltammetry, and electrochemical impedance spectroscopy (EIS).

4.1. Cyclic voltammetry

This is the most widely used electrochemical method. In this potential sweep method, the potential is varied and the current resulting from a redox event is measured. CV does not require sophisticated or expensive equipment, and moreover CV is the electrochemical technique less affected by the kinetic heterogeneity (distribution of electron transfer rates due to changes in the molecular environment of the redox reporter caused by SAM defects [57]. In other words, because of the kinetic heterogeneity, k_{ET} obtained from electrochemical measurements may contain contributions either from well-organized domains, or from those which are disordered [59]. From CV measurements one can estimate the surface coverage and k_{ET} and use further for biosensing affinity applications, since the ET rate from the redox reporter to the electrode surface may be hampered as a response to a specific binding effect and correlated with the concentration of a target analyte. The surface coverage Γ can be estimated from the slope of the dependence of I_p on the scan rate ν [37,58] and compared to a theoretical maximum based on the molecular surface area of the adsorbate as in Eq. (6) [57]:

$$I_p = \frac{n^2 F^2}{4RT} \nu A_{SUR} \Gamma \quad (6)$$

where n is the number of electrons transferred per mole of reaction, F is the Faraday constant and A_{SUR} is the surface area. The redox potential, E_0, is calculated as the average of the anodic and cathodic peak potentials, E_{pa} and E_{pc}, while the peak separation ΔE_p, is calculated as the difference $E_{pa} - E_{pc}$. The peak separation increases at high values of the scan rate, but at slow scan rates the peak separation is practically zero because the redox center is adsorbed onto the electrode and diffusion does not play a role [62,63]. The overpotential η defined as the difference $E_p - E_0$ can be used further to estimate $k_{ET,}$ since for each scan rate ν, the ET rate constant at a particular value of η ($k_s(\eta)$), can be calculated as:

$$k_s = \frac{I_p}{Q} \quad (7)$$

where Q is the total passed charge.

In the experimental setup, the initial potential is selected such that the oxidation state of the redox centers remains unchanged at the start of a scan. The potential is scanned past the formal potential E_0 to a point at which the current returns to baseline. The scan direction is then reversed and returned to the initial starting potential. In the following experiments the scan rate is varied to give a range of η values that can be used in the Tafel plot η vs. log $k_s(\eta)$ to estimate k_{ET} [64]. CV was used often either to verify the insulating properties and the integrity of SAMs [22,45,48] to calculate the influence of the peptide

macrodipole over k_{ET} and the surface coverage [23,37,40,55,61,64]. Recently, electrodes fabricated from double walled carbon nanotubes DWCNTs) were covalently loaded with Fc-modified aminoisobutyric acid peptide, and the ET rates capabilities were probed with CV. The CNT electrodes comprised of double walled CNTs (DWCNTs) demonstrated significantly higher peak current compared to their single walled counterparts (SWCNTs). This fact was attributed to a higher loading of the Fc-modified peptide to the outer wall of the nanotube, through the presence of a larger number of defects sites within the sp^2 carbon lattice for the DWCNTs [65]. The apparent ET rate constants of the Aib_5-Fc decorated DWCNT and SWCNT were calculated using Laviron's method for the condition of $\Delta E_p < 200$ mV [57]. By considering the transfer coefficient, α, to be 0.3–0.7, the average ET rate constants, k_{app}, were estimated according to the equation:

$$k_{app} = \frac{m\nu nF}{RT} \tag{8}$$

where m was s a dimensionless parameter related to the peak-to peak separation [65]. From the slope of the plot of $\nu = f(m-1)$, the term $m\nu$ was estimated and hence k_{app} determined. The k_{app}s for the DWCNT and SWCNT electrodes were $31 \pm 6\ s^{-1}$, and $23 \pm 2\ s^{-1}$, respectively. These values are comparable to ET rates reported for other redox bound vertically aligned CNT arrays on cysteamine modified gold [66]. These results indicated that DWCNTs may offer an attractive alternative to SWCNTs in building electrochemical sensors. Yet for biosensing applications involving peptide ligands, SWV is by far the voltammetric technique preserving the advantages of CV in terms of simplicity and cost-effectiveness, and also providing enhanced sensitivity [67].

4.2. Square wave- and differential pulse voltammetry

SWV is an electrochemical technique which uses a potential modulation consisting of a staircase potential ramp modified with square-shaped potential pulses [67]. At each step of the staircase ramp, two equal in height and oppositely directed potential pulses are imposed. The latter two potential pulses complete a single potential cycle in SWV. The potential cycle in SWV is repeated at each step of the staircase ramp during the SWV experiment [68]. In order to minimize the contribution of the charging current, the current sampling is performed at the end of each potential pulse. The currents associated with forward and backward potential pulses (the forward and backward components) are plotted versus the potential of the staircase ramp (the mid potential of the two neighbouring pulses composing one potential cycle). The net current (for each potential cycle) is obtained as the difference between the forward and backward currents of a single potential pulse and represents the output of a SWV voltammogram [69]. Another related voltammetric technique is differential pulse voltammetry (DPV), which uses pulses of constant amplitude superimposed on the potential linear sweep [70].The current sampling is performed just before and at the end of the modulation pulse, recording the difference as the result, in order to minimize the contribution of the charging current. As in the case of SWV, the plot of the net current vs. potential pulses represents a symmetrical peak-shaped curve [71].

The decrease or the increase of the net peak current *Ip* during SWV or DPW experiments, as response to a specific binding effect occurring at the electrode functionalized surface, expresses the basic principle of most peptide based bio- and immunoassays. For example, Li and co-workers have developed a redox-peptide immunosensor for the epidermal growth factor receptor (EGFR), based on a "signalling-on "DPV approach [11]. Here Fc-modified peptide ligands for EGFR were immobilized on a gold electrode. Upon the binding of the EGFR target, an increase of Ip was recorded as a result of increase of the rate at which the redox label collides with the electrode surface (Fig.4).

The amplitude of the current increase displayed a linear relationship with logarithm of EGFR concentrations within the range $1 \times 10^{-6} - 1 \times 10^{-10}$ g·L^{-1}, with a limit of detection (LOD) of 3.7×10^{-11} g·L^{-1} in diluted serum samples. However, this approach using immobilized redox ligand peptide is often affected by voltammetric baseline fluctuations and capacitance current [25] presumably because the ligand peptide in the unbound state cannot be considered structure-free and the secondary structure of the peptide chain cannot be controlled as in the case of, for example, short DNA oligomers [72]. To overcome these drawbacks Puiu and co-workers proposed a modular-built redox-peptide sensor, targeting the anti-deamidated gliadin peptide (DGP) antibody [24]. In this modular approach a short helical support peptide (SP) was immobilized on the surface of a gold electrode and then tagged with Methylene Blue and with a recognition peptide the alpha-2 deamidated gliadin peptide (DGP), a 33-mer peptide containing the 56–88 residues of alpha gliadin from gluten. The binding of the specific antibody to the recognition peptide decreased the efficiency with which the support peptide transferred electrons to the gold surface, leads to a SW signal decrease ("signalling-off" response) (Fig. 5).

Here a concentration of target antibody of 1 μg·mL^{-1} (6.7 nM) lead to a 22% signal suppression in diluted serum samples.

In the work of *Ding* and co-workers, self- assembled nanowires of Fc-tagged peptides (Fc-PNW) comprising the phenylalanine–phenylalanine (Phe-Phe) sequence, coated with poly(diallyl dimethyl)ammonium chloride) (PDDA) were functionalized with gold nanoparticles (AuNps) and probe antibodies (Ab_2) for a sandwich immunoassay targeting human IgG antibody [73]. The capture antibody (Ab_1) was attached onto a graphene/gold nanoparticle (AuNPs–GN) composite film (Fig. 6).

The binding of the target IgG to the capture antibody followed by the binding of Fc-PNW-Ab_2 causes a sharp increase of the peak current in the SWV assay. The Fc-peptide electrochemical immunosensor displayed a low detection limit (5 fg/mL) for human IgG and a wide linear range encompassing four orders of magnitude (from 10 fg/mL to 100 pg/mL).

4.3. Alternating current voltammetry and electrochemical impedance spectroscopy

Alternating current (AC) voltammetry, similarly to CV, is a potential sweep method [57]. A starting and ending potential are specified that index the E_0 of the redox species. Additionally, a sinusoidally oscillating AC wave is superimposed on the potential waveform. The frequency of the AC can be varied; the magnitude of the AC oscillations is small compared to the overall voltage variation [74]. The resulting AC is recorded and the electrochemical response appears as a single peak.

EIS measures the frequency response of a system by measuring the impedance, Z. To do that, a small AC signal is applied over a range of frequencies at a specified potential. Varying the frequency changes the relative contribution of each of the elements in equivalent circuit (Randles circuit model) to the overall impedance. For a ferrocene-modified peptide SAM, the Randles circuit is presented in Fig. 7. Measuring impedances over a wide range of frequencies allows the value of each individual element of the Randles circuit to be determined [75]. Here R_S is the solution resistance, CPE is the monolayer constant phase element (with $Z_{CPE} = 1/Q(i\omega)^n$, ω being the angular frequency), R_{ET} and C_{ET} are the ET resistance and capacitance, respectively [76].

AC voltammetry experiments data combined with CV and EIS output can provide the values of Γ, C_{ET}, A_{SUR} and R_S. EIS data is generally analyzed using the Nyquist plot [77]. In Nyquist (complex-plane impedance) plots, the ordinate is the imaginary axis, Z_{Im}, and the abscissa is the real axis, Z_{Re} [57,78]. The typically fitting programs provided with the potentiostat software allow the estimation of C_{ET} and R_{ET}, and hence k_{ET} using Eq. (9) [76]:

$$k_{ET} = \frac{1}{2R_{ET}C_{ET}} \tag{9}$$

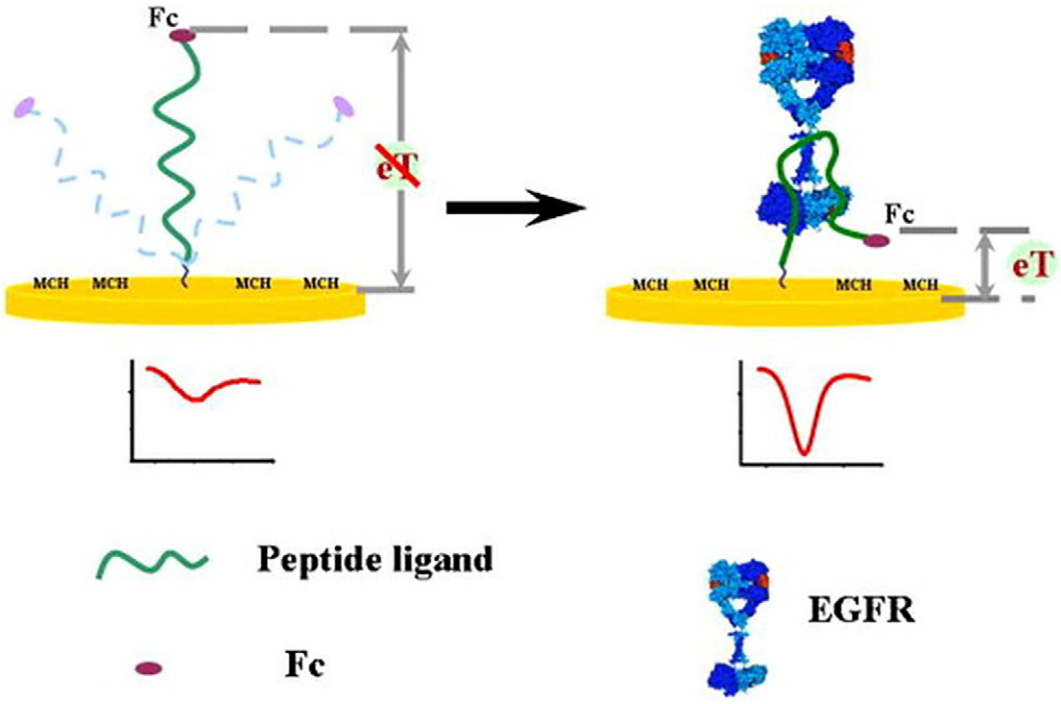

Fig. 4. Increase of the peak current at the binding of the EGFR target to the Fc-modified peptide ligand (MCH is 6-mercaptohexanol). Reproduced from [11] with permission of Elsevier.

EIS experiments can be quite useful as they allow several different parameters to be measured in one experiment. The main issues are due to the non-ideal behaviour of the system which can dramatically alter the values obtained from analysis based on the Randles circuit model. These drawbacks can be solved by providing additional elements to the Randles circuit [62]. AC voltammetry is used for typical "signalling on "or signalling off" peptide based-assays for antibody detection [25] since the analytical AC response is a peak-shaped curve much alike to SW- and DPV outputs. In contrast to these techniques, AC voltammetry and EIS are much more time-consuming. Swisher and co-workers have recently reported an" signalling-off" peptide-based biosensor for measuring the activity of proteases using nanoelectrode arrays (NEAs), fabricated with vertically aligned carbon nanofibers (VACNFs) of around 150 nm in diameter and 3–5 μm in length [79]. Here, two Fc-tagged tetrapeptides specific to cancer-mediated proteases legumain and cathepsin B were immobilized onto VACNFs. The redox signal of Fc was measured with AC voltammetry at around 1 kHz frequency on VACNF/NEAs. This particularly enhanced ACV signal was net superior to the ACV output obtained with macroscopic glassy carbon electrodes, due to the inherent conductive properties of VACNFs. The kinetic parameters of the proteolytic cleavage of the surface-attached tetrapeptides by proteases were estimated through ACV measurements.

5. Recent achievements in the biosensing area

Besides their use as scaffolds and mimics, redox-tagged peptides are remarkably robust and versatile building blocks for the preparation of peptide and protein conjugates, displaying electrochemical sensing properties [21,56,80]. In such systems, Fc or MB act as the redox reporters, while the peptide or protein bridge, plays the role of the recognition element that engages in specific interactions with the target [21]. Fc and MB tagged peptides/proteins are mostly used in affinity assays for enzyme and antibodies [24,25]. Moreover, acyclic and cyclic-Fc-peptides were reported as promising electrochemical sensors for metal ions and anions, in which the appearance of additional redox waves indicates the presence of a tight host–guest complex [21,81].

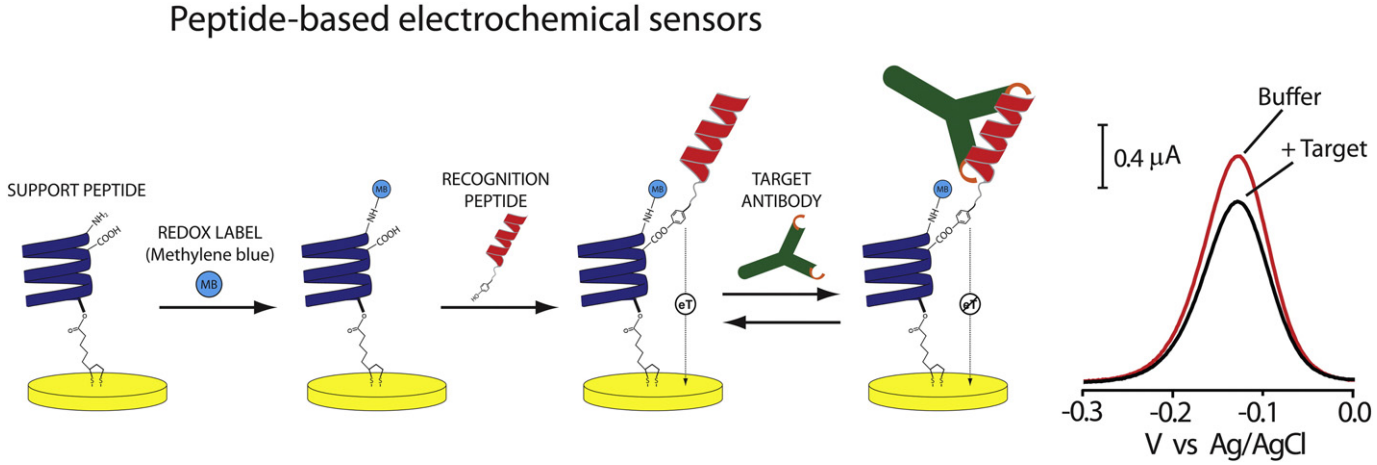

Fig. 5. Decrease of the net current at the target binding to recognition peptide grafted onto redox-modified peptide support. Reproduced from [24] with permission of RSC Publishing.

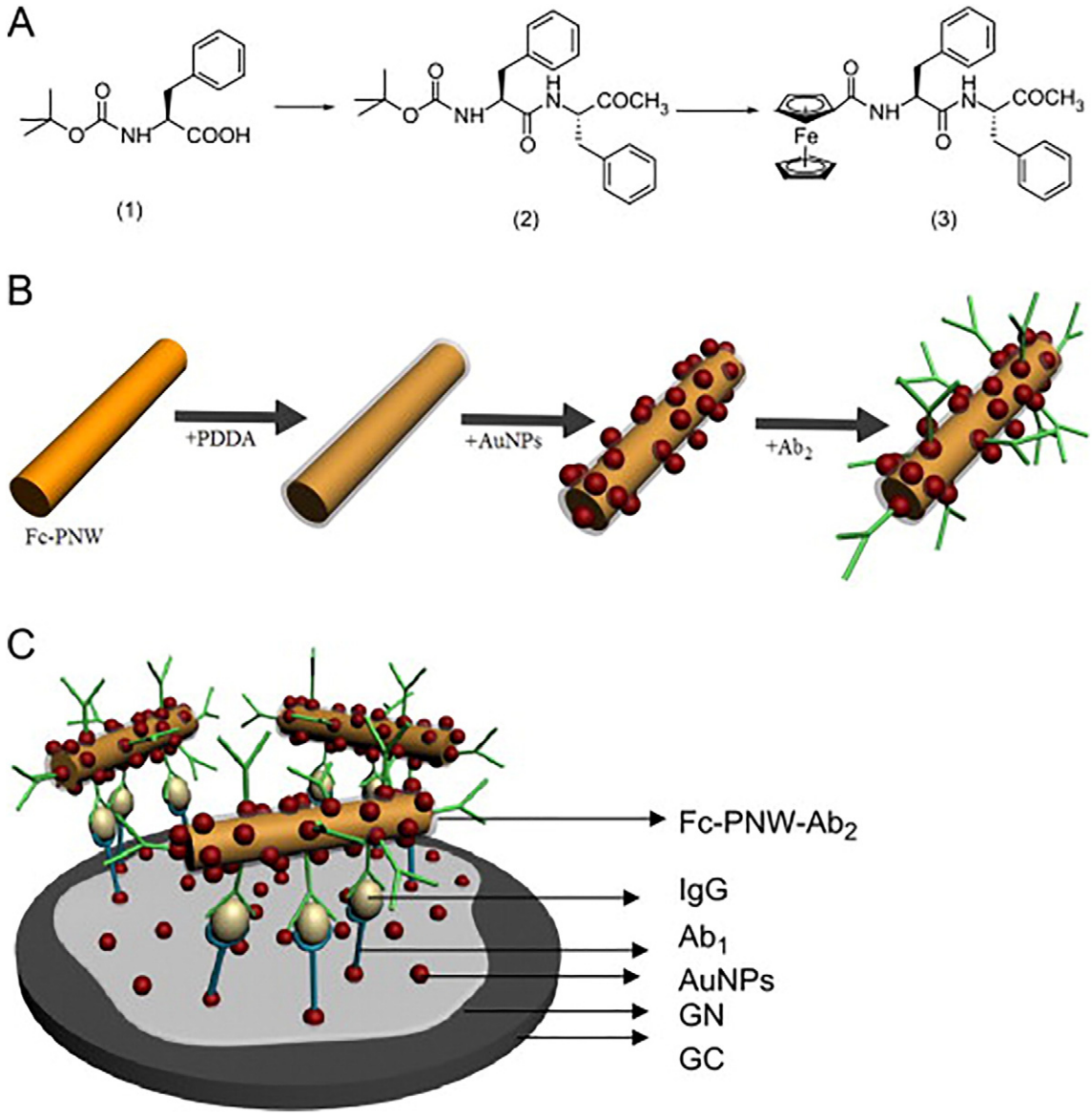

Fig. 6. Schematic representation for the synthesis of Fc-Phe-Phe-OMe (A), for the preparation of Fc-PNW-Ab_2 (B) and the immunosensor (C). Reproduced from [73] with permission of Elsevier.

Simple non-tagged short peptides proved their ability to act as selective ligands for cations such as copper [29,82]. A brief overview of the latest achievements for electrochemical peptide-based sensors is presented in Table 1.

6. Conclusions and outlook

The past decade witnessed a burst of applications for peptide-based sensors, particularly in the clinical diagnosis area, with promising perspective for implementation in point-of-care platforms. Electrochemical transducers coated with conductive peptide nanocomposite are able to store non-antibody recognition elements and may be amenable to miniaturized, easy-to-use and portable devices. Despite the great progress achieved, several issues still remain: the total number of non-antibody recognition elements developed/discovered is still significantly lower than that of antibodies and biosensing assays based on peptide ligands/recognition elements have been drastically confined by the non-specific binding of target molecules, resulting in significantly reduced sensitivity, especially for clinical samples [26]. Besides that, peptide materials have to meet several criteria: the materials should afford economically scale up and reproducible material production, purification, processing and long-term storage; they should be chemically compatible with aqueous solutions and physiological conditions [3]. We have offered herein a short overview of the most used electrochemical methods in the evaluation of conductive properties of peptidic films with application in the biosensing area. We are hoping that our work will assist researchers in their advance for design and development of peptide-based sensors for biological and clinical applications.

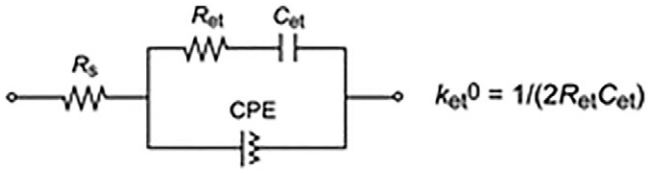

Fig. 7. Randles circuit for analyzing ACV and EIS data obtained with Fc-peptide SAM. Adapted from [76] with permission of ACS publication.

Table 1
Electrochemical peptide-based sensors with peptide ligands for relevant biological targets.

Target	Assay	Immobilized peptide	Redox tag	Electrochemical method	Analytical/kinetic performance	Transducer	Ref.
Matrix metalloproteinase-9 (MMP-9)	Enzymatic	GPLGMWSRC	MB	CV	Linear range: 1pM-1 nM LOD = 7 pM	Au	[83]
Trypsin	Enzymatic	GRPS-PEG disulfide	Fc	CV	Dynamic range: 25 ng/mL to 100 μg/mL $k_{cat} = 1.1 \times 10^{-2}$ s^{-1} $K_M = 7.6$ nM	Au	[84]
α- thrombin	Enzymatic	RFSRPQL-PEG disulfide	Fc	CV	Dynamic range: 25 ng/mL to 100 μg/mL $k_{cat} = 1.0 \times 10^{-2}$ s^{-1} $K_M = 10$ nM	Au	
Plasmin	Enzymatic	KTKTC	Fc	DPV	LOD = 50 ng/mL $k_{cat}/K_M = 63$ nM^{-1} s^{-1}	Au	[85]
Epidermal growth factor receptor	Affinity	YHWYGYTPQNVI	Fc	DPV	Linear range LOD = 3.7×10^{-11} g/L.	Au	[11]
Prostate specific antigen	Affinity	HSSKLQL	2-hydroxy-naphtoquinone	SWV	Dynamic range: 1pM -1 nM	Glassy carbon modified with 4-azidoaniline	[86]
Amyloid 1–42	Affinity	RGTWEGKWK	Fc	SWV	LOD = 240pM	Au	[87]
HIV anti-p24 antibody	Affinity	EAAEWDRVHP	MB	ACV	LOD = 10 nM	Au	[25]
Legumain	Enzymatic	H_2N-$(CH_2)_4$-CO-AAAN-NH-CH_2–	Fc	ACV	$k_{cat}/K_M = 4.3 \times 10^4$ M^{-1} s^{-1}	VACNFs deposited on a Cr-coated Si chip	[79]
Cathepsin B	Enzymatic	H_2N-$(CH_2)_4$-CO-LRFG-NH-CH_2-	Fc	ACV	$k_{cat}/K_M = 1.13\ 3 \times 10^4$ M^{-1} s^{-1}		
SW620 colorectal carcinoma cells	Affinity	DDAGNRQP	–	EIS	Linear range 2.0×10^2–2.0×10^8 cells/mL LOD = 79 cells/mL	Au	[88]

Acknowledgement

This work was supported by a grant of Ministry of Research and Innovation, CNCS - UEFISCDI, project number PN-III-P4-ID-PCE-2016-0288.

Conflict of interest

None.

Author contributions

Both M. P. and C. B have equally conceived, written and edited this manuscript.

References

[1] E. Kokkoli, A. Mardilovich, A. Wedekind, E.L. Rexeisen, A. Garg, J.A. Craig, Self-assembly and applications of biomimetic and bioactive peptide-amphiphiles, Soft Matter 2 (2006) 1015–1024.
[2] A. Lakshmanan, S. Zhang, C.A.E. Hauser, Short self-assembling peptides as building blocks for modern nanodevices, Trends Biotechnol. 30 (2012) 155–165.
[3] Y. Loo, S. Zhang, C.A.E. Hauser, From short peptides to nanofibers to macromolecular assemblies in biomedicine, Biotechnol. Adv. 30 (2012) 593–603.
[4] A.L. Boyle, E.H.C. Bromley, G.J. Bartlett, R.B. Sessions, T.H. Sharp, C.L. Williams, P.M.G. Curmi, N.R. Forde, H. Linke, D.N. Woolfson, Squaring the circle in peptide assembly: from fibers to discrete nanostructures by de novo design, J. Am. Chem. Soc. 134 (2012) 15457–15467.
[5] L. Adler-Abramovich, E. Gazit, The physical properties of supramolecular peptide assemblies: from building block association to technological applications, Chem. Soc. Rev. 43 (2014) 6881–6893.
[6] B.J. Pepe-Mooney, R. Fairman, Peptides as materials, Curr. Opin. Struct. Biol. 19 (2009) 483–494.
[7] M. Kai, K. Takeda, T. Morita, S. Kimura, Distance dependence of long-range electron transfer through helical peptides, J. Pept. Sci. 14 (2008) 192–202.
[8] E. Gazit, Self-assembled peptide nanostructures: the design of molecular building blocks and their technological utilization, Chem. Soc. Rev. 36 (2007) 1263–1269.
[9] A. McQuistan, A.J. Zaitouna, E. Echeverria, R.Y. Lai, Use of thiolated oligonucleotides as anti-fouling diluents in electrochemical peptide-based sensors, Chem. Commun. 50 (2014) 4690–4692.
[10] M.S. Mannoor, S. Zhang, A.J. Link, M.C. McAlpine, Electrical detection of pathogenic bacteria via immobilized antimicrobial peptides, Proc. Natl. Acad. Sci. U. S. A. 107 (2010) 19207–19212.
[11] R. Li, H. Huang, L. Huang, Z. Lin, L. Guo, B. Qiu, G. Chen, Electrochemical biosensor for epidermal growth factor receptor detection with peptide ligand, Electrochim. Acta 109 (2013) 233–237.
[12] H. Chen, S. Jia, J. Zhang, M. Jang, X. Chen, K. Koh, Z. Wang, Sensitive detection of copper(ii) ions based on the conformational change of peptides by surface plasmon resonance spectroscopy, Anal. Methods 7 (2015) 8942–8946.
[13] B.S. Flavel, M. Nambiar, J.G. Shapter, Electrochemical detection of copper using a Gly-Gly-his modified carbon nanotube biosensor, SILICON 3 (2011) 163–171.
[14] R.V. Ulijn, A.M. Smith, Designing peptide based nanomaterials, Chem. Soc. Rev. 37 (2008) 664–675.
[15] R.S. Vieira-Pires, J.H. Morais-Cabral, 3_{10} helices in channels and other membrane proteins, J. Gen. Physiol. 136 (2010) 585–592.
[16] D. Papapostolou, A.M. Smith, E.D.T. Atkins, S.J. Oliver, M.G. Ryadnov, L.C. Serpell, D.N. Woolfson, Engineering nanoscale order into a designed protein fiber, Proc. Natl. Acad. Sci. U. S. A. 104 (2007) 10853–10858.
[17] R.V. Ulijn, V. Jayawarna, A. Smith, J.E. Gough, Hydrogel compositionsGoogle Patents 2013.
[18] J. Gao, C. Tang, M.A. Elsawy, A.M. Smith, A.F. Miller, A. Saiani, Controlling self-assembling peptide hydrogel properties through network topology, Biomacromolecules 18 (2017) 826–834.
[19] J. Wang, X. Zhao, J. Li, X. Kuang, Y. Fan, G. Wei, Z. Su, Electrostatic assembly of peptide nanofiber–biomimetic silver nanowires onto graphene for electrochemical sensors, ACS Macro Lett. 3 (2014) 529–533.
[20] E. Chow, J.J. Gooding, Peptide Modified Electrodes as Electrochemical Metal Ion Sensors, Electroanalysis 18 (2006) 1437–1448.
[21] S. Martic, M. Labib, P.O. Shipman, H.-B. Kraatz, Ferrocene-peptido conjugates: from synthesis to sensory applications, Dalton Trans. 40 (2011) 7264–7290.
[22] G.A. Orlowski, S. Chowdhury, H.-B. Kraatz, Reorganization energies of ferrocene-peptide monolayers, Langmuir 23 (2007) 12765–12770.
[23] J. Juhaniewicz, S. Sek, Peptide molecular junctions: distance dependent electron transmission through oligoprolines, Bioelectrochemistry 87 (2012) 21–27.
[24] M. Puiu, A. Idili, D. Moscone, F. Ricci, C. Bala, A modular electrochemical peptide-based sensor for antibody detection, Chem. Commun. 50 (2014) 8962–8965.
[25] J.Y. Gerasimov, R.Y. Lai, An electrochemical peptide-based biosensing platform for HIV detection, Chem. Commun 46 (2010) 395–397.

[26] H. Chen, J. Huang, A. Palaniappan, Y. Wang, B. Liedberg, M. Platt, A.I.Y. Tok, A review on electronic bio-sensing approaches based on non-antibody recognition elements, Analyst 141 (2016) 2335–2346.
[27] J. Slaninová, V. Mlsová, H. Kroupová, L. Alán, T. Tůmová, L. Monincová, L. Borovičková, V. Fučík, V. Čeřovský, Toxicity study of antimicrobial peptides from wild bee venom and their analogs toward mammalian normal and cancer cells, Peptides 33 (2012) 18–26.
[28] M. Szardenings, Phage display of random peptide libraries: applications, limits, and potential, J. Recept. Signal Transduct. Res. 23 (2003) 307–349.
[29] S. Pavan, F. Berti, Short peptides as biosensor transducers, Anal. Bioanal. Chem. 402 (2012) 3055–3070.
[30] G. Guidotti, L. Brambilla, D. Rossi, Cell-penetrating peptides: from basic research to clinics, Trends Pharmacol. Sci. 38 (2017) 406–424.
[31] A.M. Hung, S.I. Stupp, Simultaneous self-assembly, orientation, and patterning of peptide−amphiphile nanofibers by soft lithography, Nano Lett. 7 (2007) 1165–1171.
[32] K.H. Smith, E. Tejeda-Montes, M. Poch, A. Mata, Integrating top-down and self-assembly in the fabrication of peptide and protein-based biomedical materials, Chem. Soc. Rev. 40 (2011) 4563–4577.
[33] H.-D. Yu, M.D. Regulacio, E. Ye, M.-Y. Han, Chemical routes to top-down nanofabrication, Chem. Soc. Rev. 42 (2013) 6006–6018.
[34] H. Matsui, P. Porrata, G.E. Douberly, Protein tubule immobilization on self-assembled monolayers on au substrates, Nano Lett. 1 (2001) 461–464.
[35] I.A. Banerjee, L. Yu, H. Matsui, Location-specific biological functionalization on nanotubes: attachment of proteins at the ends of nanotubes using au nanocrystal masks, Nano Lett. 3 (2003) 283–287.
[36] Y.-T. Long, E. Abu-Irhayem, H.-B. Kraatz, Peptide electron transfer: more questions than answers, Chem. Eur. J. 11 (2005) 5186–5194.
[37] E. Gatto, M. Venanzi, A. Palleschi, L. Stella, B. Pispisa, L. Lorenzelli, C. Toniolo, F. Formaggio, G. Marletta, Self-assembled peptide monolayers on interdigitated gold microelectrodes, Mater. Sci. Eng. C 27 (2007) 1309–1312.
[38] M. Lauz, S. Eckhardt, K.M. Fromm, B. Giese, The influence of dipole moments on the mechanism of electron transfer through helical peptides, Phys. Chem. Chem. Phys. 14 (2012) 13785–13788.
[39] P. Gobbo, S. Antonello, I. Guryanov, F. Polo, A. Soldà, F. Zen, F. Maran, Dipole moment effect on the electrochemical desorption of self-assembled monolayers of 310-Helicogenic peptides on gold, ChemElectroChem 3 (2016) (1964–1964).
[40] H.S. Mandal, H.-B. Kraatz, Electron transfer across α-helical peptides: potential influence of molecular dynamics, Chem. Phys. 326 (2006) 246–251.
[41] M. Zhang, J. Zhao, H. Yang, P. Liu, Y. Bu, 310-helical peptide acting as a dual relay for charge-hopping transfer in proteins, J. Phys. Chem. B 117 (2013) 6385–6393.
[42] A.M. Smith, S.F.A. Acquah, N. Bone, H.W. Kroto, M.G. Ryadnov, M.S.P. Stevens, D.R.M. Walton, D.N. Woolfson, Polar assembly in a designed protein fiber, Angew. Chem. Int. Ed. 44 (2005) 325–328.
[43] L. Zhang, J. Hermans, 310 helix versus .alpha.-helix: a molecular dynamics study of conformational preferences of Aib and alanine, J. Am. Chem. Soc. 116 (1994) 11915–11921.
[44] S. Bezer, M. Matsumoto, M.W. Lodewyk, S.J. Lee, D.J. Tantillo, M.R. Gagne, M.L. Waters, Identification and optimization of short helical peptides with novel reactive functionality as catalysts for acyl transfer by reactive tagging, Org. Biomol. Chem. 12 (2014) 1488–1494.
[45] E. Gatto, A. Porchetta, M. Scarselli, M. De Crescenzi, F. Formaggio, C. Toniolo, M. Venanzi, Playing with peptides: how to build a supramolecular peptide nanostructure by exploiting helix···helix macrodipole interactions, Langmuir 28 (2012) 2817–2826.
[46] M. Sisido, S. Hoshino, H. Kusano, M. Kuragaki, M. Makino, H. Sasaki, T.A. Smith, K.P. Ghiggino, Distance dependence of Photoinduced electron transfer along α-helical polypeptides, J. Phys. Chem. B 105 (2001) 10407–10415.
[47] P. Siddarth, R.A. Marcus, Comparison of experimental and theoretical electronic matrix elements for long-range electron transfer, J. Phys. Chem. 94 (1990) 2985–2989.
[48] K. Kitagawa, T. Morita, S. Kimura, Electron transport properties of helical peptide dithiol at a molecular level: scanning tunneling microscope study, Thin Solid Films 509 (2006) 18–26.
[49] F. Polo, S. Antonello, F. Formaggio, C. Toniolo, F. Maran, Evidence against the hopping mechanism as an important electron transfer pathway for conformationally constrained oligopeptides, J. Am. Chem. Soc. 127 (2005) 492–493.
[50] S.W. Feldberg, Implications of Marcus−hush theory for steady-state heterogeneous electron transfer at an inlaid disk electrode, Anal. Chem. 82 (2010) 5176–5183.
[51] R.A. Marcus, N. Sutin, Electron transfers in chemistry and biology, Biochim. Biophys. Acta Rev. Biomembr. 811 (1985) 265–322.
[52] H.B. Gray, J.R. Winkler, Long-range electron transfer, Proc. Natl. Acad. Sci. U. S. A. 102 (2005) 3534–3539.
[53] M.E. Ener, H.B. Gray, J.R. Winkler, Hole hopping through tryptophan in cytochrome P450, Biochemistry 56 (2017) 3531–3538.
[54] A. Nitzan, Electron transmission through molecules and molecular interfaces, Annu. Rev. Phys. Chem. 52 (2001) 681–750.
[55] B.R. Chaudhry, J.D.E.T. Wilton-Ely, A.B. Tabor, D.J. Caruana, Effect of peptide orientation on electron transfer, Phys. Chem. Chem. Phys. 12 (2010) 9996–9998.
[56] H.S. Mandal, H.-B. Kraatz, Electron transfer mechanism in helical peptides, J. Phys. Chem. Lett. 3 (2012) 709–713.
[57] A.L. Eckermann, D.J. Feld, J.A. Shaw, T.J. Meade, Electrochemistry of redox-active self-assembled monolayers, Coord. Chem. Rev. 254 (2010) 1769–1802.
[58] A.J. Wain, H.N.L. Do, H.S. Mandal, H.-B. Kraatz, F. Zhou, Influence of molecular dipole moment on the redox-induced reorganization of α-helical peptide self-assembled monolayers: an electrochemical SPR investigation, J. Phys. Chem. C 112 (2008) 14513–14519.
[59] J. Juhaniewicz, J. Pawlowski, S. Sek, Electron transport mediated by peptides immobilized on surfaces, Isr. J. Chem. 55 (2015) 645–660.
[60] H.O. Finklea, D.D. Hanshew, Electron-transfer kinetics in organized thiol monolayers with attached pentaammine(pyridine)ruthenium redox centers, J. Am. Chem. Soc. 114 (1992) 3173–3181.
[61] A. Heck, P.B. Woiczikowski, T. Kubař, B. Giese, M. Elstner, T.B. Steinbrecher, Charge transfer in model peptides: obtaining Marcus parameters from molecular simulation, J. Phys. Chem. B 116 (2012) 2284–2293.
[62] A.J. Bard, L.R. Faulkner, Electrochemical Methods: Fundamentals and Applications, 2nd Edition John Wiley & Sons, 2000.
[63] C.G. Zoski, Handbook of Electrochemistry, Elsevier, 2007.
[64] S. Okamoto, T. Morita, S. Kimura, Electron transfer through a self-assembled monolayer of a double-helix peptide with linking the terminals by ferrocene, Langmuir 25 (2009) 3297–3304.
[65] K.E. Moore, B.S. Flavel, J. Yu, A.D. Abell, J.G. Shapter, Increased redox-active peptide loading on carbon nanotube electrodes, Electrochim. Acta 89 (2013) 206–211.
[66] B.S. Flavel, J. Yu, A.V. Ellis, J.G. Shapter, Electroless plated gold as a support for carbon nanotube electrodes, Electrochim. Acta 54 (2009) 3191–3198.
[67] J.H. Reeves, S. Song, E.F. Bowden, Application of square wave voltammetry to strongly adsorbed quasireversible redox molecules, Anal. Chem. 65 (1993) 683–688.
[68] V. Mirceski, R. Gulaboski, M. Lovric, I. Bogeski, R. Kappl, M. Hoth, Square-wave voltammetry: a review on the recent progress, Electroanalysis 25 (2013) 2411–2422.
[69] V. Mirceski, S. Komorsky-Lovric, M. Lovric, Square-Wave Voltammetry: Theory and Application, Springer, Berlin Heidelberg, 2007.
[70] J.G. Osteryoung, R.A. Osteryoung, Square Wave Voltammetry, Anal. Chem. 57 (1985) 101A–110A.
[71] X. He, Q. Zhu, F. Liao, L. Zhu, Z. Ai, Differential pulse Voltammetric determination and application of square-wave voltammetry of yRNA on a CPB-cellulose modified electrode, Electroanalysis 19 (2007) 1375–1381.
[72] F. Ricci, A.J. Bonham, A.C. Mason, N.O. Reich, K.W. Plaxco, Reagentless, electrochemical approach for the specific detection of double- and single-stranded DNA binding proteins, Anal. Chem. 81 (2009) 1608–1614.
[73] Y. Ding, D. Li, B. Li, K. Zhao, W. Du, J. Zheng, M. Yang, A water-dispersible, ferrocene-tagged peptide nanowire for amplified electrochemical immunosensing, Biosens. Bioelectron. 48 (2013) 281–286.
[74] F. Scholz, Electroanalytical Methods: Guide to Experiments and Applications, Springer, Berlin Heidelberg, 2009.
[75] E. Katz, I. Willner, Probing biomolecular interactions at conductive and semiconductive surfaces by impedance spectroscopy: routes to impedimetric immunosensors, DNA-sensors, and enzyme biosensors, Electroanalysis 15 (2003) 913–947.
[76] Y. Arikuma, K. Takeda, T. Morita, M. Ohmae, S. Kimura, Linker effects on monolayer formation and long-range electron transfer in helical peptide monolayers, J. Phys. Chem. B 113 (2009) 6256–6266.
[77] S.E. Creager, T.T. Wooster, A new way of using ac voltammetry to study redox kinetics in electroactive monolayers, Anal. Chem. 70 (1998) 4257–4263.
[78] M. Dong, H. Qi, S. Ding, M. Li, Electrochemical determination of trypsin using a heptapeptide substrate self-assembled on a gold electrode, Microchim. Acta 182 (2015) 43–49.
[79] L.Z. Swisher, L.U. Syed, A.M. Prior, F.R. Madiyar, K.R. Carlson, T.A. Nguyen, D.H. Hua, J. Li, Electrochemical protease biosensor based on enhanced AC voltammetry using carbon nanofiber nanoelectrode arrays, J. Phys. Chem. C 117 (2013) 4268–4277.
[80] Q. Liu, J. Wang, B.J. Boyd, Peptide-based biosensors, Talanta 136 (2015) 114–127.
[81] P.D. Beer, S.R. Bayly, Anion Sensing by Metal-Based Receptors, in: I. Stibor (Ed.), Anion Sensing: −/−, Springer Berlin Heidelberg, Berlin, Heidelberg 2005, pp. 125–162.
[82] W. Yang, E. Chow, G.D. Willett, D.B. Hibbert, J.J. Gooding, Exploring the use of the tripeptide Gly-Gly-His as a selective recognition element for the fabrication of electrochemical copper sensors, Analyst 128 (2003) 712–718.
[83] J. Lee, J.Y. Yun, W.C. Lee, S. Choi, J. Lim, H. Jeong, D.-S. Shin, Y.J. Park, A reference electrode-free electrochemical biosensor for detecting MMP-9 using a concentric electrode device, Sensors Actuators B Chem. 240 (2017) 735–741.
[84] J. Adjémian, A. Anne, G. Cauet, C. Demaille, Cleavage-sensing redox peptide monolayers for the rapid measurement of the proteolytic activity of trypsin and α-thrombin enzymes, Langmuir 26 (2010) 10347–10356.
[85] K. Ohtsuka, I. Maekawa, M. Waki, S. Takenaka, Electrochemical assay of plasmin activity and its kinetic analysis, Anal. Biochem. 385 (2009) 293–299.
[86] I. Strzemińska, S. Sainte Rose, G. Fanchine, S. Anquetin, V. Reisberg, M.C. Noël, B. Pham, Piro, grafting of a peptide probe for prostate-specific antigen detection using diazonium electroreduction and click chemistry, Biosens. Bioelectron. 81 (2016) 131–137.
[87] H. Li, Y. Cao, X. Wu, Z. Ye, G. Li, Peptide-based electrochemical biosensor for amyloid β 1–42 soluble oligomer assay, Talanta 93 (2012) 358–363.
[88] L. Han, P. Liu, V.A. Petrenko, A. Liu, A label-free electrochemical impedance Cytosensor based on specific peptide-fused phage selected from landscape phage library, Sci. Rep. 6 (2016) 22199.